Available online at www.sciencedirect.com
SCIENCE DIRECT®
Deep-Sea Research I 51 (2004) 1441–1455
DEEP-SEA RESEARCH PART I
www.elsevier.com/locate/dsr

Rectilinear and circular inertial motions in the Western Mediterranean Sea

Hans van Haren[a,*], Claude Millot[b]

[a]Department of Physical Oceanography, Royal Netherlands Institute for Sea Research (NIOZ), P.O. Box 59, 1790 AB Den Burg, The Netherlands
[b]Antenne LOB-COM-CNRS, c/o IFREMER, BP 330, F-83507 La Seyne-sur-mer, France

Received 22 March 2004; accepted 2 July 2004

Abstract

Kinetic energy spectra appeared similar at all observational depths in the 3000 m deep Algerian Basin, Western Mediterranean Sea. They were featureless except for a single peak at ~2% above the local inertial frequency (f), even at depths (z) where stratification was very weak, $N(z) = O(f)$. At great depths a second peak was observed at ~0.99f. However, at a single point, we observed rotary spectra varying considerably with stratification and depth. Where $N < f$, that is between 600 and 1200 m in a series of homogeneous layers associated with a double diffusion process and below 2200 m in a dense homogeneous water formed nearby, all near-inertial horizontal motions were almost rectilinear. The observation of near-rectilinear inertial motions was in contrast with common observations of near-circularly polarized inertial motions, which were found, for example, from the same mooring at depths where $N \geqslant 2.5f$, that is in continuously stratified waters encountered near the surface (100 m) and at intermediate depths (1800 m). Our observations suggested that the near-inertial motions in the Algerian Basin did not always represent internal gravity waves, but also dominant inertio (gyroscopic) waves. These waves could have been generated after excitation of the surface layer by atmospheric disturbances and the surface pressure gradient (barotropic) excitation of a simple 2-layer model via a coastal boundary condition, a process common in shelf seas.

Keywords: Algerian Basin; Near-inertial motions; Internal gravity and gyroscopic waves

1. Introduction

Horizontal currents (u, v) oscillating at frequencies (σ) close to the local inertial frequency $f = 2\Omega \sin\varphi$ (φ denoting the latitude and $\mathbf{\Omega}$ the Earth's rotational vector) are dominant in large parts of the Mediterranean Sea, with amplitudes of $O(10^{-1}\,\mathrm{m\,s^{-1}})$, whilst tidal motions have amplitudes of $O(10^{-3}\,\mathrm{m\,s^{-1}})$ (Albérola et al., 1995; Tsimplis et al., 1995). As a result, the Mediterranean Sea is an excellent site to study potential

*Corresponding author. Fax: +31-222-319674.
E-mail address: hansvh@nioz.nl (H. van Haren).

0967-0637/$ - see front matter © 2004 Elsevier Ltd. All rights reserved.
doi:10.1016/j.dsr.2004.07.009

deep-sea mixing caused by internal wave motions that are not predominantly forced by tides.

Motions at frequencies close to f ('near-inertial' motions) near the sea surface are mainly generated by atmospheric disturbances (e.g. Pollard and Millard, 1970; Millot and Crépon, 1981; D'Asaro and Perkins, 1984; Kundu, 1993). However, enhanced near-inertial energy can be found at great depths (Webster, 1968; Perkins, 1972; Fu, 1981; van Haren et al., 2002). It is often suggested that most near-inertial energy is transported downwards into the ocean interior via propagating waves satisfying an internal wave dispersion relation (Kroll, 1975; Leaman and Sanford, 1975; D'Asaro and Perkins, 1984; Garrett, 2001; Maas, 2001). With $N=(-g/\rho\partial\rho/\partial z)^{0.5}$ denoting the buoyancy frequency and for $N\gg f_{\mathrm{eff}}=f+\zeta/2$ the 'effective' inertial frequency (Mooers, 1975; Kunze, 1985), which includes vorticity ζ due to sub-inertial motions, propagating internal gravity waves exist only in the range $f_{\mathrm{eff}}<\sigma<N$. As a result, near-inertial internal gravity waves in most stratified conditions have frequencies just above the local effective inertial frequency. Although we suppose in the following that $\zeta=0$ for simplicity, all results can be generalized to $\zeta\neq 0$.

1.1. Waves and mixing in the ocean interior

During downward propagation, near-inertial waves are important for mixing as most destabilizing vertical shear $\mathbf{S}=(\partial u/\partial z,\partial v/\partial z)$ is found at near-inertial frequencies (e.g. Pinkel, 1983). However, D'Asaro (1991) suggests that high wave number near-inertial waves, generating largest shear, cannot propagate very far from their source near the surface before dissipating. Thus, we need an explanation for observed intermediate and deep near-inertial shear. In the ocean, this motivated studies on near-inertial motions that are locally generated, via parametric sub-harmonic instability (PSI) of low wave number motions at frequencies $2f$, either from storms generated far poleward (Nagasawa et al., 2000) or predominantly near $|\varphi|\approx 29^{\circ}$ where $2f=M_2$, the dominant tidal frequency (Hibiya et al., 2002).

Here, we focus on the (internal wave) character of near-inertial current observations from the surface to great depths (~3000 m) in the Algerian Basin of the Western Mediterranean Sea (Fig. 1). In this confined basin, one does not expect high wave number near-inertial motions generated by PSI, because it is neither 'connected' to ocean regions around $\varphi\approx 29^{\circ}$N, nor large enough to comprise both near-inertial motions generated at arbitrary f and at the latitude φ' corresponding to $2\Omega\sin\varphi'=2f$. Furthermore, in our study area, deep stratification can become very weak ($N<2f$ and even $N\sim 0$), as we inferred from present (Fig. 2) and previous data (Perkins, 1972). As a result, the classical internal wave range $f<\sigma<N$ that is found under the approximation of neglecting the horizontal component of the Earth's rotation vector no longer applies. Under this approximation, propagating internal gravity waves, approaching layers where $N<f$, will be reflected into the layer where $N>f$, whilst only evanescent waves (having exponentially decaying amplitudes) can exist in the layer where $N<f$. However, in weak stratification the horizontal component of the Earth's rotation vector ($2\Omega\cos\varphi$) becomes more important for the generation of inertio-gravity (also called

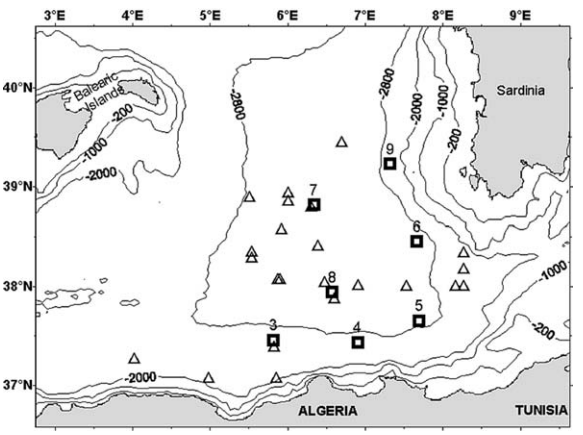

Fig. 1. Site of moorings (□, numbered 3–9) during project 'ELISA' between July 1997 and 1998. CTD casts down to the bottom are indicated by 'Δ'. They were obtained during ELISA campaigns in July/August 1997 and March 1998, and during the ADIOS campaign in March 2001.

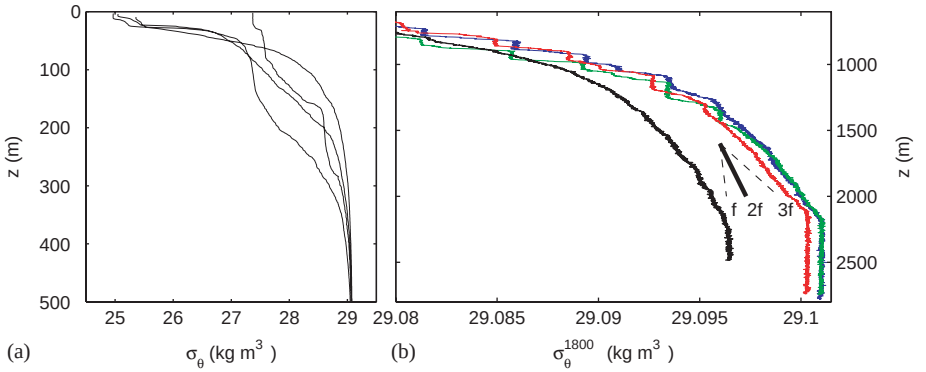

Fig. 2. Four examples (of 23 stations in total, cf. Fig. 1) of potential density-depth profiles obtained using CTD in the Algerian Basin: (a) 0–500 m with potential density referenced to the surface. (b) The lower 2200 m of the profiles. The short sloping lines indicate density stratification yielding $N = f$, $3f$ (dashed lines) and $N = 2f$ (heavy solid line). The profile offset to the left of the short sloping lines is from the Algerian Margin. Potential density is referenced to 1800 m.

gyroscopic-gravity) waves (Saint-Guily, 1970; Gascard, 1973; LeBlond and Mysak, 1978; Brekhovskikh and Goncharov, 1994). In the limit for $N = 0$, the momentum equations yield solutions for pure inertio (gyroscopic) internal waves.

1.2. Inertio-gravity waves

To better understand the links between the frequency (σ) and the wave number vector ($\mathbf{k}$) of internal inertio-gravity waves, and to describe their propagation character, we consider the general wave solutions provided by e.g. LeBlond and Mysak (1978) in the range:

$$\begin{aligned}
&\sigma_{\text{low}} < \sigma < \sigma_{\text{high}},\\
&\sigma_{\text{low}} = 2\Omega(\sin^2\varphi\cos^2\nu - (\sin 2\varphi \sin 2\nu)/2\\
&\qquad + (\cos^2\varphi + (N/2\Omega)^2)\sin^2\nu)^{0.5},\\
&\sigma_{\text{high}} = 2\Omega(\sin^2\varphi\sin^2\nu + (\sin 2\varphi \sin 2\nu)/2\\
&\qquad + (\cos^2\varphi + (N/2\Omega)^2)\cos^2\nu)^{0.5}\\
&\qquad \text{for } \nu = \text{atan}(\sin 2\varphi/(\cos 2\varphi\\
&\qquad + (N/2\Omega)^2))/2.
\end{aligned} \tag{1}$$

With these frequency bounds the inertio-gravity wave dispersion relation adopts the form

$$(N^2 - \sigma^2)\kappa_1^2 + (\sigma_{\text{high}}^2 - \sigma^2)\kappa_2^2 + (\sigma_{\text{low}}^2 - \sigma^2)\kappa_3^2 = 0 \tag{2}$$

in the rotated wave number coordinates (κ_1, κ_2, κ_3), defined by

$$\begin{pmatrix}\kappa_1\\ \kappa_2\\ \kappa_3\end{pmatrix} = \begin{pmatrix}1 & 0 & 0\\ 0 & \cos\nu & \sin\nu\\ 0 & -\sin\nu & \cos\nu\end{pmatrix}\begin{pmatrix}k_1\\ k_2\\ k_3\end{pmatrix}, \tag{3}$$

where $(k_1, k_2, k_3) = \mathbf{k}$ the wave number vector in the earth Cartesian coordinates (x, y, z).

It is easily verified that, for $N \gg f$, $\nu \approx 0$, $\sigma_{\text{low}} \approx f$, $\sigma_{\text{high}} \approx N$, and $(\kappa_1, \kappa_2, \kappa_3) \approx (k_1, k_2, k_3)$. In that case in (2), which is the equation of a cone, the factors of κ_1^2 and κ_2^2 are similar, and both have a sign (+) opposite to (and are much larger than) that of the factor of κ_3^2, for $\sigma \approx f$. As a result, for near-inertial motions the wave number vector can be found along a relatively sharp cone centered on the κ_3-axis $\approx (z, -\mathbf{g})$-axis, with a (near-circular) ellipse in the (x, y) plane (Fig. 3). As the group-velocity (energy) vector $\boldsymbol{c}_{\text{g}}$ can be found by differentiating (2) with respect to κ_i, $i = 1, 2, 3$,

$$\boldsymbol{c}_{\text{g}} = \frac{1}{\sigma\kappa^2}[(N^2 - \sigma^2)\kappa_1, (\sigma_{\text{high}}^2 - \sigma^2)\kappa_2, (\sigma_{\text{low}}^2 - \sigma^2)\kappa_3], \tag{4}$$

$\boldsymbol{c}_{\text{g}} \perp \boldsymbol{\kappa}$, with opposite signs for their 'vertical' components κ_3 as $\sigma_{\text{low}} < \sigma$. For $\sigma \approx f$ this vector lies on a wide (near-circular) ellipse cone,

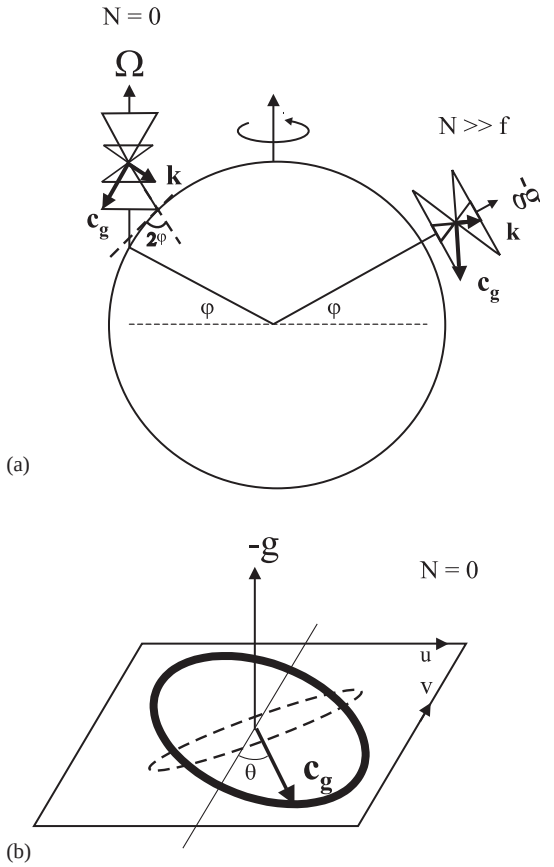

Fig. 3. (a) Impression of different propagation surfaces for internal waves at constant frequency $\sigma \approx f$ for varying stratification at particular latitude φ. When $N \gg f$ (depicted to the right), the cone of wave number (and phase speed) is narrow, so that the wave number vector $\mathbf{k}$ is nearly in the direction of gravity. The wave group speed (and energy propagation) vector $\boldsymbol{c}_g$ lies on cones perpendicular to the wave number cones, so that in this case they are very wide and circular motions lying in this plane are nearly horizontal. When $N = 0$ (depicted to the left, for clarity), f is further away from the internal wave bounds (1) and the wave number cone is (much) wider (and the wave group cone much narrower). In this gyroscopic limit the plane of particle motions can be strongly inclined with respect to gravity. (b) As a result, the projection of the circular hodograph (thick line) of gyroscopic internal motions on the local horizontal plane (u, v) can result in a near-rectilinear elliptical hodograph (dashed line). In the Mediterranean, near-inertial gyroscopic motions coming from the North-East have their major axis directed NW–SE (theoretically).

so that the near-circular near-inertial particle displacements projected on an (x, y) plane are also observed near-circular (Fig. 3).

When N decreases, and as long as $\sigma_{\text{low}} < \sigma < N < \sigma_{\text{high}}$, v becomes $\neq 0$, the wave number vector cone widens following (2), whilst in the (κ_1, κ_2)-plane it becomes more elliptical and its κ_3-vector rotates away from $-\mathbf{g}$ (by $v \approx 9^\circ$ for $N = 2.5f$). When N is so low that $\sigma_{\text{low}} < N < \sigma < \sigma_{\text{high}}$, the sign of the κ_1^2 factor in (2) changes, so that the opposite sign becomes that of κ_2^2 and the wave number cone is centered on the κ_2-axis. In the limit $N = 0$, $v = \varphi$, $\sigma_{\text{low}} = 0$, $\sigma_{\text{high}} = 2\Omega$, gravity no longer dominates and the wave number vectors associated with pure gyroscopic waves lie in cones centered on the Earth's rotational vector, i.e. their axis is strongly inclined at an angle $(90 - \varphi)^\circ$ from $-\mathbf{g}$ (Fig. 3). From (2), the factors for κ_1 and κ_3 are identical, implying a circle in the hodograph of motions for all frequencies in the range $0 < \sigma < 2\Omega$ for purely north–south propagating waves, and $0 < \sigma < f$ for purely east–west propagating waves (Saint-Guily, 1970). For $\sigma \approx f$, following (4), this circle lies in the plane tilted with respect to the horizontal at an angle θ between

$$0^\circ \leqslant \theta \leqslant 2\varphi \tag{5}$$

so that the projection to the (x, y)-plane can vary between a circular and a near-rectilinear hodograph (the two extremes are for north–south propagation) (Fig. 3). Pure rectilinear horizontal near-inertial gyroscopic motions are expected at $\varphi = 45^\circ$. Coincidentally, the direction of the projected non-circular current ellipse allows one to infer the direction of energy propagation of gyroscopic waves. For example, a down- and southeastward propagating wave would give a northeast–southwest directed major axis of the ellipse. Such determination of energy propagation is more difficult for near-inertial internal gravity waves that exhibit near-circular horizontal motions.

Pure gyroscopic waves have similar properties as internal gravity waves, like $\mathbf{c}_g \perp \mathbf{k}$, but with the same signs for their 'vertical' components κ_2, following (4). However, at the latitude of the Algerian Basin, f is near the middle of the pure gyroscopic internal wave frequency band, whilst near-inertial motions are very close to the low-frequency bound of internal gravity waves (for $N \gg f$). For a typical (Algerian Basin) intermediate value of $N = 2.5f \approx 3\Omega$, the theoretical inertio-gravity wave band is between $0.87f < \sigma < 1.15N$.

1.3. Background conditions

In the Algerian Basin, the occurrence of such low stratification at intermediate depths varies between the mooring sites although it is present everywhere below 2200 m (Fig. 2). This is due to the general circulation in the area that, therefore, must be specified. To compensate for the water deficit in the Mediterranean Sea and due to rotation, Atlantic water flows alongslope and anticlockwise in the whole sea forming a 200-m surface layer (Millot, 1999). In the study area, it forms the 50-km wide Algerian Current that, being unstable, generates 100-km anticyclonic eddies a few times per year. These eddies can extend down to the bottom (~3000 m) and have a two-layer structure (Millot et al., 1997). They provide additional vorticity of 0.1–0.2f in the upper 300 m and of 0.01–0.02f in the remainder of the water column. They propagate downstream at a few km d^{-1} up to the entrance of the channel of Sardinia where, being too large and too deep, they tend to follow the deep isobaths. Hence, they separate from their parent current and describe an anticlockwise circuit roughly along the 2800 m isobath in the whole study area (Puillat et al., 2002). When passing off Sardinia, they entrain seaward relatively warm and salty intermediate waters, which originated from the Levantine Basin (between 200 and 600 m) and from the Tyrrhenian Basin (600–2000 m) (Millot, 1999; Millot and Taupier-Letage, 2004). Below 2000 m (the depth of the channel of Sardinia), relatively cool and fresh water reside originating from the Liguro-Provençal Basin just to the north (MEDOC Group, 1970).

Consequently, Levantine water is dispatched from Sardinia (mainly over mooring 6, Fig. 1) and spread in the basin interior (mainly towards moorings 7 and 8) while rarely being encountered close to Algeria (at moorings 3–5), except in a strongly modified form. Because this water generates a marked double diffusion process in the water below (Fuda et al., 2000), a series of homogeneous layers develop, strongly varying in both time and space (mainly due to eddies passing by). For instance, the isolated profile in Fig. 2b is characteristic of the Algerian margin with well-mixed intermediate waters between 1200 and 2200 m and the homogeneous Liguro-Provençal water (formed during wintertime convection) below. The other profiles in Fig. 2b are characteristic of the mooring 6 surroundings with step-like structures 100 m thick below the Levantine water (600–1400 m), the layer of continuously varying density associated with the Tyrrhenian water (1400–2200 m) and the deep homogeneous water (>2200 m). As a result, stratification strongly varies spatially in the Algerian Basin, making it appropriate for studying the effects of stratification on near-inertial motions and the effects of near-inertial motions on internal waves.

1.4. Outline

We focus on observations from mooring 6, close to the channel of Sardinia, showing most distinct layers of different rotary current properties associated with different stratification during a period without eddies passing by. The other data sets were analyzed for comparison, but are not shown. Spectral observations as at mooring 6 were found similar at moorings 5, 7 and 9. However, the observations at these moorings were less clear than at mooring 6, for example occurring during shorter periods (2 months at mooring 7) and with less vertical correlation (at mooring 5). In contrast, at moorings 3, 4 and 8 further away from the Channel of Sardinia and closer to the Algerian coastal Current, rotary current properties changed more gradually with depth, evidence of a smooth density profile without steps there (Fig. 2).

2. Data handling

Hourly data were obtained in the Algerian Basin using different Aanderaa RCM current meters (Fig. 1) during project 'ELISA' between July 1997 and 1998. Mooring 6 consisted of 5 current meters at 100 m (RCM-7), 350 m (RCM-9), 1000 m (RCM-8), 1800 m (RCM-5), and an RCM-8 at 100 m above the bottom ($H \approx 2800$ m depth). The RCM-9 did not work correctly and its data are not considered further. For the other RCMs, the velocity (V) is calculated from the number of

revolutions (R) of a rotor during one sampling interval for an RCM5 or from the vector-averaged (50 times per sampling interval) speed for an RCM7,8 according to $V = a + bR$, so that no revolutions lead to $V = a$, the starting velocity. Each instrument was just below 2 Benthos spherical floats and the main buoyancy element of ~400 kg net was on top of the mooring. Data sections varied in length between 125 and 270 days. Here, we used the common data section of ~125 days, between 22 October 1997 and 1 March 1998 when there were no passages of meso-scale eddies at the investigated mooring site, so that the vertical displacement of the top of mooring 6 was less than 10 m. Low-frequency, sub-inertial motions were mainly caused following passages of atmospheric disturbances.

We performed kinetic and rotary spectral analysis using various degrees of freedom, balancing between frequency resolution and (random) statistical significance. Relative changes in kinetic energy levels are compared with CTD-estimates of $N(z)$. As suggested (Garrett and Munk, 1972; henceforth GM) for internal wave band frequencies well away from boundaries $f \ll \sigma \ll N$: power $P(\sigma) \sim N\sigma^p$, with slope p varying between $-2.5 < p < -1.5$. For the rotary spectra we used the method by Gonella (1972), who decomposed (East, North) oscillatory current components (u, v) into rotary current components

$$w_+ = \frac{\tilde{u} - \mathrm{i}\tilde{v}}{2} = W_+ \exp(-\mathrm{i}\theta_+)$$

the anti-clockwise rotary component (6a)

$$w_- = \frac{\tilde{u} + \mathrm{i}\tilde{v}}{2} = W_- \exp(\mathrm{i}\theta_-),$$

the clockwise rotary component (6b)

for harmonic $\tilde{u} = U \exp(\mathrm{i}\varphi_u)$ and similarly for $\tilde{v}$, which combines $(u, v) = (U\cos(\sigma t - \varphi_u), V\cos(\sigma t - \varphi_v))$ into one complex current

$$w = u + \mathrm{i}v = w_+^* \exp(\mathrm{i}\sigma t) + w_- \exp(-\mathrm{i}\sigma t), \quad (7)$$

where ()* denotes a complex conjugate, $\mathrm{i}^2 = -1$ and σ is the harmonic frequency. Any horizontal current ellipse is a sum of the two rotary components (6), so that a rectilinear oscillatory motion can be composed of rotary components having equal amplitudes. Defining rotary amplitude spectra

$$P_+(\sigma) = \langle w_+ \rangle^* \langle w_+ \rangle / 2$$

the anti-clockwise spectrum, (8a)

$$P_-(\sigma) = \langle w_- \rangle^* \langle w_- \rangle / 2 \quad \text{the clockwise spectrum,} \quad (8b)$$

the brackets denoting Fourier transform, so that the kinetic energy spectrum is

$$P_{\mathrm{KE}}(\sigma) = P_-(\sigma) + P_+(\sigma). \quad (9)$$

The polarization of the horizontal current ellipses is inferred from the 'rotary coefficient'

$$C_{\mathrm{R}}(\sigma) = |P_-(\sigma) - P_+(\sigma)| / P_{\mathrm{KE}}(\sigma), \quad (10)$$

$C_{\mathrm{R}} = 0$ for pure rectilinear motion and 1 for pure circular motion. Under symmetric forcing C_{R} simplifies

$$C_{\mathrm{R}}(\sigma) = \frac{|\langle W_-^2 \rangle - \langle W_+^2 \rangle|}{\langle W_-^2 \rangle - \langle W_+^2 \rangle} = \frac{2\langle UV \sin(\varphi_u - \varphi_v) \rangle}{\langle U^2 + V^2 \rangle} = \frac{2\sigma f}{\sigma^2 + f^2} = \frac{2e}{1 + e^2}, \quad (11)$$

where $e = (W_+ - W_-)/(W_+ + W_-)$ is the eccentricity of the horizontal current ellipse. Note from (11) that for internal gravity waves under conditions $N \gg f$, $C_{\mathrm{R}}(N) \approx 0$ and $C_{\mathrm{R}}(f) \approx 1$. Although pure circular polarization is found for all $0 < \sigma < 2\Omega$ gyroscopic waves in their plane of propagation, their projection on the (x, y)-plane may vary strongly (Fig. 3). In the Algerian Basin, minimum gyroscopic eccentricity $e_{\min}(f) = 0.23$ is expected following (5), yielding $C_{\mathrm{R}}(f) \approx 0.43$ using (11).

This difference in polarization for different N at fixed frequency (f) is verified using observations below.

3. Observations

3.1. Kinetic energy spectra

At mooring 6, kinetic energy spectra (Fig. 4) demonstrated the importance of near-inertial motions in the Mediterranean Sea, from the surface to the bottom. Besides the dominant

near-inertial peak, the spectra generally showed a featureless sloping continuum in the internal wave band (Fig. 4a). Near-inertial peak frequencies $\sigma_p = (1.02 \pm 0.02)f$ did not vary significantly with depth (Fig. 4b), except at 2700 m (where $\sigma_p \approx (0.99 \pm 0.02)f$, with a broader band centered around $0.97f$ and a second peak at $1.02f$). Although some peak frequencies at 2700 m were different from the other depths, these were not associated with σ_{low}, since $N \approx 0$ (Fig. 2). Likewise, $\sigma_p(1800) \neq \sigma_{low}(N \approx 3\Omega)$. The uncertainty in σ_p was attributable to frequency resolution following spectral smoothing. However, the visible finite band around σ_p in Fig. 4 reflected the near-inertial 'intermittency', the (strong) variation in amplitude with time resulting in typically 10 inertial periods in a group (van Haren, 2004b). Note that the width of the near-inertial peak did not vary with depth (except being broader at 2700 m).

In contrast, entire spectra varied with depth by a factor that was more or less constant in frequency (especially spectra of 100 and 1800 m in Fig. 4a), except for a dependency on the dominance of internal waves (see discussion below on spectral slopes). We noted that the spectrum at 1800 m was least energetic at most frequencies. Sub-inertial currents were very similar below 1000 m (time series not shown), with a difference between 1800 and 2700 m mainly in amplitude, by a factor of 1.25 in favor of the latter.

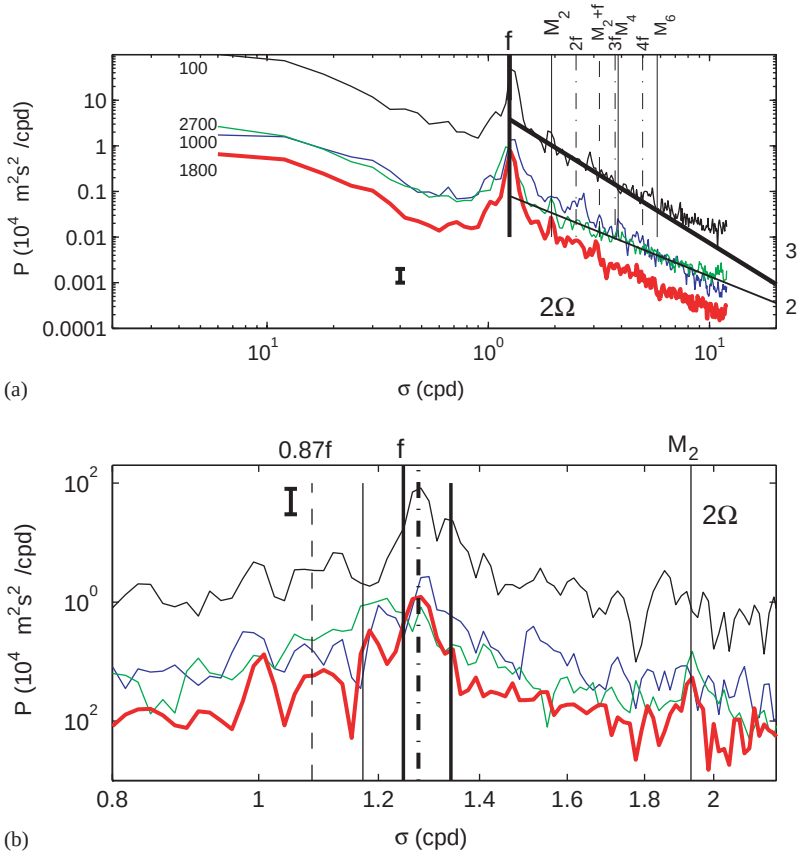

Fig. 4. (a) Kinetic energy spectra from 4 months of current meter observations at 100 m (black), 1000 m (blue), 1800 m (red) and 2700 m (green) at mooring 6. The number of degrees of freedom $\nu \approx 26$df, so that the effective fundamental band width $\Delta\sigma_f = 0.1$ cpd, leading to the 95% significance confidence interval as indicated by the vertical bar. For $\sigma > f$ the spectrum at 100 m approached a constant sloping $P(\sigma) \propto \sigma^{-3}$ (indicated by slope '−3'), at 2700 m $P(\sigma) \propto \sigma^{-2}$('−2'). (b) Detail of nearly raw ($\nu \approx 5$ df) version of (a), with the dash–dotted line indicating $1.02f$. Solid lines are at $0.94f$, f, $1.07f$, M_2.

At 1800 and 2700 m, a semidiurnal tidal peak emerged from the internal wave band continuum. The weak amplitudes of these tidal motions and the polarization of the horizontal current ellipses (see below) suggested a predominantly barotropic motion. This motion was apparently weaker than the internal wave band continuum at 100 and 1000 m. This description of kinetic energy spectral variation with depth was found for all moorings. Further comparison between different spectra is discussed below.

3.2. Rotational properties

Despite the similar shape of the kinetic energy spectra, rotational properties of the horizontal motions at f and in the internal wave band varied strongly with depth, most clearly at mooring 6 (Fig. 5). Only at the upper current meter (100 m) we observed $C_R(\sigma)$ resembling (11) typical for (symmetrically forced) internal gravity waves. At 1000 and 2700 m $C_R(\sigma \geqslant f) \leqslant 0.4$, implying in the mean near-rectilinear motions and/or motions of randomly varying phase at all 'internal wave band' frequencies. For $\sigma \approx f$ we found a mean $C_R = 0.25 \pm 0.1$ (at 1000 m) and $C_R = 0.3 \pm 0.1$ (2700 m), so that mean eccentricity $e(f) = 0.13 \pm 0.05$ (1000 m) and $e(f) = 0.16 \pm 0.05$ (2700 m). These values are somewhat lower than the minimum values predicted following (5). At 1800 m we found $C_R(f) = 0.9$, C_R gradually decreasing with frequency like (11) albeit at somewhat lower values and best representing (11) near interaction frequencies like $M_2 + f$ for $\sigma > 2f$ (Fig. 5c). Although such interaction was weak here (due to the weak tides) in comparison to other regions, e.g. near continental slopes (van Haren et al., 2002; Xing and Davies, 2002), this suggested importance of non-linear interaction in the internal wave band. Such interaction can be between barotropic and baroclinic motions (van Haren et al., 2002). Here, the dip in polarization at the semidiurnal tidal band was evidence of barotropic motions.

The above vertical variation of polarization of internal wave band motions was also clear from raw data (u, v)-hodographs (Fig. 6a–d) that were dominated by sub- and near-inertial motions. The latter followed a near-circular path at 100 m (Fig. 6a) and 1800 m (Fig. 6c) and near-rectilinear paths directed roughly NNW–SSE (major axis varying $\pm 20°$) at 1000 m (Fig. 6b) and 2700 m (Fig. 6d). Although evident in the raw data, this was more clearly seen in near-inertial band-pass filtered data (Fig. 6e–h). The near-rectilinear motions were basically aligned with the deep sub-inertial current, and to within the above variations with topography (Fig. 1). With the variations in major axis directions we also noted variations in polarization, varying between $0.01 < e(f) < 0.3$, so that $0.05 < C_R(f) < 0.55$ (Fig. 6f, h). At 1000 and 2700 m we noted slightly larger current amplitudes than at 1800 m and, in the raw data (Fig. 6b,d), visible starting velocities due to rotor stalling. The latter amounted ~20% of the data at 1000 m, and <3% at 2700 m.

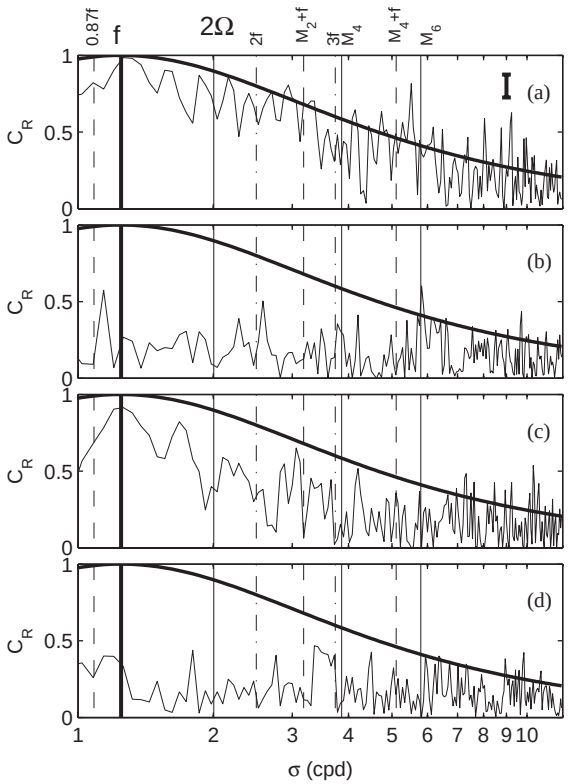

Fig. 5. Moderately smoothed ($\nu \approx 26$df) rotary coefficient spectra for the records in Fig. 2, for (a) 100 m, (b). 1000 m, (c) 1800 m, (d) 2700 m. In (a) the 95% significance confidence interval is indicated by the vertical bar. The smooth curves indicate theory (11).

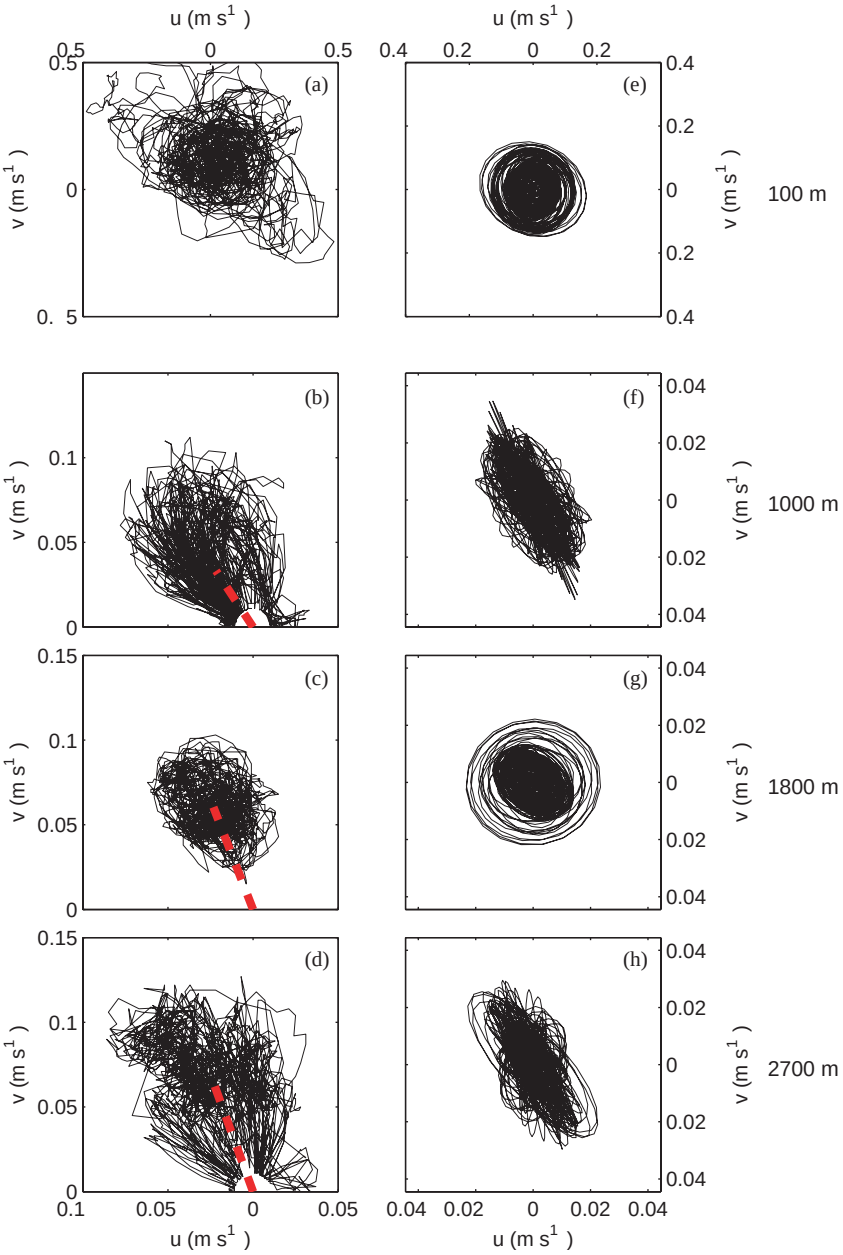

Fig. 6. Hodographs from the entire raw data records for: (a) 100 m (Note different scale from the others), (b) 1000 m, (c) 1800 m, (d) 2700 m. Horizontal axes of (b) and (c) are given in (d). (e)–(h) as (a)–(d), but for near-inertial band-pass filtered data, using sharp elliptic filters back and forth with cut-off frequencies at 0.90*f*, 1.10*f*. The heavy-dashed lines in (b)–(d) indicate the mean currents.

Rotor stalling is typically found in areas with weak currents and in areas with rectilinear oscillatory (tidal) currents during periods of weak sub-inertial motions. The starting velocities were completely absent at 1800 m (Fig. 6c) where the same (albeit somewhat weaker) sub-inertial currents were observed. Hence, the near-rectilinear currents were not due to instrumental errors.

Owing to the relatively small amount of data points affected by rotor stalling, the near-inertial motions and the spectra were not flawed (except perhaps for some influence on higher inertial harmonic frequencies at 1000 m, as discussed below).

3.3. Additional observations

Coherency with motions at 100 m was found significant for the near-inertial clockwise rotary component at 1000 and 1800 m, whilst being insignificant at all other frequencies (Fig. 7). The mean phase difference for $W_{-}(f)$ between 100 and 1000 m was $100 \pm 10^{\circ}$ and between 100 and 1800 m it was $170 \pm 10^{\circ}$ (Fig. 7b). Between 100 and 2700 m the coherence was insignificant. The observed significant near-inertial coherency suggested a simple vertical structure across a relatively large vertical distance, as reported previously (Perkins, 1972). Note that, although results may be ambiguous by one or more complete cycles of 360°, the near-inertial motions were related over large depths despite the varying polarization at different depths.

In spite of the general lack of vertical coherency at all the frequencies except f, the ratio of kinetic energy spectra at 100 and 1800 m reflected $N(z)$, not just for the internal wave continuum, as in GM, but also for the near-inertial peak height and sub-inertial frequencies. Referring to Fig. 2, we estimated N near the depths of the current meters: $N(100\,\mathrm{m}) = N_{100} = (150 \pm 50)f$, $N(600-1400\,\mathrm{m}) = N_{1000} < 10f$, $N(1400-2200\,\mathrm{m}) = N_{1800} = (2.5 \pm 0.3)f$ and $N(>2200\,\mathrm{m}) = N_{2700} = 0$. The transition between the latter two was abrupt near 2200 m in all observed profiles, suggesting a 'minimum stratification' $N = 2.5f$ for internal gravity waves, as discussed in Section 4.

The above N-values were used to scale the observed kinetic spectra and we found $P_{1800} = N_{1800}/N_{100}P_{100}$, within the 95% significance bounds for $\sigma < 3f$. Such (internal wave) scaling was only found at depths where permanent well-mixed layers ($N = 0$) were absent: at the two other depths (1000 and 2700 m), for which the above scaling did not apply, the spectra were anomalous. These spectra showed more or less the same energy content, despite different N when computed across large vertical scales of $O(100\,\mathrm{m})$. In detail, the two spectra were different in the internal wave band, as the spectrum at 1000 m showed enhancements around inertial harmonic frequencies, f, $2f$, $3f$ (shoulder to a peak at M_4), $4f$, which were less energetic at 2700 m. Partially, these higher harmonics were artificial due to the slightly weaker sub-inertial motions in association with rectilinear near-inertial motions as may be verified using a simple model (van Haren, 2004a).

However, as other higher harmonics emerged (M_4) and as the peak near $2f$ was wider than near f, they could also partially be due to changes in background conditions (van Haren, 2004a) reflected in the intermittent variation in near-inertial amplitude (Fig. 6). Furthermore, the spectral slope at 1000 m was relatively flat between $1.3f < \sigma < 2f$ ($p_{1000} = -1.3 \pm 0.2$), becoming steeper at higher frequencies (Table 1) and approaching the value $p = -3$, which was also observed at 100 and 1800 m. At 2700 m the slope remained $p = -1.9 \pm 0.2$ for the entire 'internal wave' band. These differences were associated with differences in N. $N(1000\,\mathrm{m})$ varied strongly with time, because step layer depths and thickness passing the current meter varied with time (Fig. 2b).

4. Discussion

The observed near-inertial peak blue-shift in frequency in the Algerian Basin, the same at all depths except at 2700 m (Fig. 4b), was similar to the mean value $(1.023 \pm 0.006)f$ observed at 3800 m (1000 m above the bottom) in the Bay of Biscay (van Haren, 2004b). Like Perkins (1972), who found a near-inertial peak frequency of $1.03f$ independent of depth, we found no indication for Doppler shift or relative vorticity causing the observed blue-shift in near-inertial peak frequency. Perkins (1972) also reported a gradual decrease of polarization with increasing depth, with notable exception of enhanced circular polarization at 1700 m, and a 180° phase difference between near-inertial motions at 700 and 1700 m. To explain this simple vertical structure of his observations, Perkins used an internal gravity

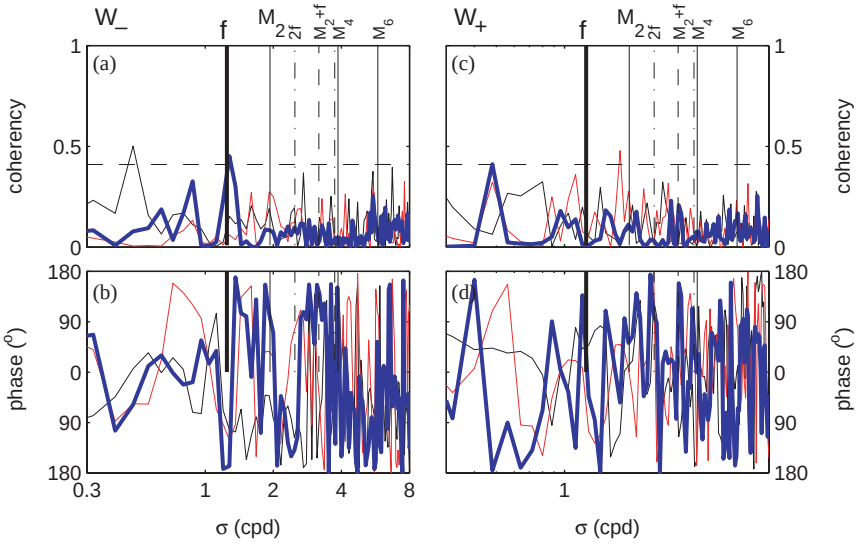

Fig. 7. (a) Coherency and (b) phase for moderately smoothed ($\nu \approx 35$df) spectra for the clockwise rotary current components between 100 and 1000 m (black), 100 and 2700 m (red) and 100 and 1800 m (blue). (c) and (d) are coherency and phase spectra for the anti-clockwise component.

Table 1
Least-square fit of spectral slope p for three different frequency bands ($\Delta\sigma$), well excluding the influence of a near-inertial peak ($\sigma > 1.3f$) and instrumental noise ($\sigma > 8f$) computed for weakly smoothed spectra ($\nu \approx 26$df)

Depth (m) $\Delta\sigma$	$1.3f < \sigma < 2f$	$1.3f < \sigma < 3f$	$1.3f < \sigma < 8f$
100	−3.6	−2.9	−2.5
1000	−1.1	−2.3	−2.8
1800	−2.8	−2.8	−2.3
2700	−1.6	−1.7	−1.9

One standard deviation is 0.2, for all slopes.

wave model fitted for the Algerian Basin. This model did neither include the gravest, barotropic mode nor gyroscopic waves, which we will consider below. Hence, Perkins' model cannot explain our observations of strong changes in polarization with depth.

4.1. Internal gravity and gyroscopic waves (coupling)

Our observed coherence between the clockwise components at 100 and 1800 m suggested large-scale coupling between near-inertial motions near the surface and those at intermediate depths, whilst 'crossing' layers of $N = 0$ around 1000 m. Our interpretation of rectilinear near-inertial motions at the latter depth (and at 2700 m) implies the first open ocean observations of gyroscopic waves using horizontal current meters. Given the observed coherence, a smooth transition between internal gravity and gyroscopic waves is suggested.

The apparent (baroclinic) mode-1 vertical structure (inferred from the observed 180° phase difference) resembled near-inertial motions generated in shallow seas. There, surface layer response and *barotropic* (mode-0) response through a coastal boundary condition lead to a 180° phase difference between the surface and the deep layer. Such response occurred 'instantaneously' after the wind onset and well before the arrival of any baroclinic near-inertial wave signal (Millot and Crépon, 1981). Adopting their shallow seas slab-layer model for the Algerian Basin, with two layers of thickness $h_1 = 300$ m and $h_2 = 2500$ m (Fig. 2a), explains more or less the amplitude decrease by a factor of ~9 between 100 and 1800 m (Fig. 6). The initial instantaneous barotropic response may resemble a (theoretical) Kelvin wave generating

(near-rectilinear) motions parallel to the steep topography across external Rossby scales of O(1000 km) from the coast. As observations below 300 m showed amplitudes, polarization and (moderately) major axis direction changing with depth and noting that moorings 3–6 and 9 were 1–2 internal Rossby radii (30–50 km, using the above layer thickness and density difference from Fig. 2a) from the coast, the barotropic response was (rapidly) modified and/or replaced by internal wave response. For $N \geqslant 2.5f$, the apparent 'minimum permanent stratification', this response was associated with internal gravity waves, possibly generated from fronts as in shallows seas where the water in the coastal region is well-mixed (Davies and Xing, 2002).

At depths where $N = 0$ this baroclinic response did not develop. At such depths gyroscopic waves were important, following our interpretation of the observed near-rectilinear motions in the horizontal plane evidence of circular particle motions in a plane at an acute (up to $2\varphi = 77^\circ$) angle to the horizontal (Fig. 3b). The observed similarity in near-inertial amplitudes at 1800 and 2700 m suggests a smooth transition between internal gravity and gyroscopic wave regimes, with little reflection at layers where $N = f$ as in traditional approaches. This is understood, as both wave types are solutions of the same non-hydrostatic equation resulting in a joint dispersion relation. This leaves possibilities for smooth transitions to adaptations in amplitude when motions move from one conical plane to the other (Fig. 8). Following (2), varying N implies a rotation of the cones, and with it the location of the group velocity vector on a particular cone, as schematically depicted. As a result, the plane of motions varies with respect to the horizontal.

Future studies should establish whether these waves are generated locally or remotely. Such modeling is beyond the scope of our paper. A recently obtained preliminary result from an analytical model (Maas, pers. comm. 2003) demonstrates the possibility of such transition. Moreover, the model shows that for meridional- and downward transport a transition from $N \sim 3f$ to a layer $N = 0$ is 100% transparent (transmitting) for waves at the inertial frequency, whilst the

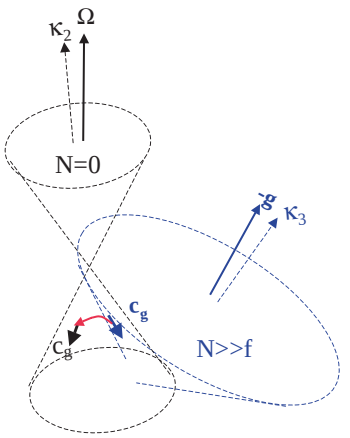

Fig. 8. Impression of (a portion) of different energy propagation surfaces for internal waves at constant frequency $\sigma \approx f$ for varying stratification. When N varies from $N \gg f$ to $N = 0$, the (blue) energy-cone around the vertical wave number axis (pointing in the direction opposite to gravity) gradually narrows and turns away from $-\mathbf{g}$ until $N = f$ (the degenerate case). For smaller N, the (black) energy-propagation cone is around the κ_2-axis near the Ω-axis of the Earth's rotation and exactly matching that for $N = 0$. It is assumed that the above sketched transition in N results in a smooth change of energy propagation vector, for example along a path like sketched with the red arrow.

plane of motions has an angle of 2φ as in (5). The transmission rapidly decreases to 0% at $\sigma = 2\Omega$, demonstrating the importance of near-inertial motions. Zonal propagation yields more complex (not yet available) results.

From the observed direction 155–335° ± 20° of the major current ellipse axes at 1000 and 2700 m (Fig. 6) we inferred an energy source area in the direction 65° ± 20° (or 180° to the opposite). The shelf slope is found to the NE of mooring 6 (Fig. 1), implying not maximum inclination of the plane of motions, different from our observations. In fact, we occasionally observed almost rectilinear motions that are not possible following gyroscopic wave theory. However, speculating, these may reflect superposition of plane gyroscopic waves from different sources. Such sources may be near the Algerian coastal shelf, where large scale eddies (with vorticity $\zeta \neq 0$) resided during the observations, implying different (effective) inertial frequency, possibly explaining the anomalous near-inertial peaks observed at 2700 m.

The occasionally observed small eccentricity $e = 0.05$ suggests a (perfect) Kelvin wave, as suggested for tidal currents in the North Sea near the British coast (LeBlond and Mysak, 1978). However, we rule this out as a possibility to explain our observations, because such wave was not observed at the intermediate (stratified) depths and because shelf slopes are not vertical walls so that Kelvin waves in practice show strongly polarized motions. Also, it is demonstrated that rectilinear tidal motions in the central North Sea are due to a superposition of two highly polarized Poincaré waves.

4.2. Minimum stratification

Our observations suggest that the aforementioned minimum stratification and coastal boundary conditions were imperative for the local development of circular near-inertial horizontal motions. For example, at 1000 m periods of gyroscopic waves developing in homogeneous layers ($N \approx 0$), alternated with periods of free internal gravity waves developing when stratified interfaces ($N \gg f$) passed the current meter. In the mean however, the steps prevented the development of near-inertial horizontal circular motions, associated with internal gravity waves.

A similar strong influence of near-coastal stratification was observed on the polarization of tidal currents in shallow seas (Visser et al., 1994) and on the development of near-inertial motions in shelf seas in general: such motions were not found in wintertime well-mixed conditions (van Haren, 2000). In shelf seas, a minimum permanent stratification was also needed to support near-inertial shear associated with circular near-inertial motions. Our observations suggest this also holds for the Algerian Basin, although not necessarily to support high-frequency internal waves.

Stabilizing large-scale stratification and destabilizing shear appeared more or less in equilibrium, and our estimate of the gradient Richardson number $Ri = N^2/|\mathbf{S}|^2 \approx 1$: we observed $|\mathbf{S}| \approx 1f$ (1800–2700 m), but assuming all *horizontal* near-inertial internal gravity wave shear was across depths where $N \approx 2.5f$ (1800–2200 m; Fig. 2b) we computed $|\mathbf{S}| \approx 2.2f$. Note that such shear magnitude varied on slow, sub-inertial time scales. Such marginal dynamical stability was also observed across extremely strong stratification in the North Sea (van Haren et al., 1999). Eriksen (1978) and Munk (1981) suggested $Ri \approx 1$ typical for a saturated internal wave field, in equilibrium with $N(z)$. The absence of slowly varying shear below 2200 m may be related with gyroscopic waves, that show circular motions in planes strongly inclined to the horizontal, and with them a shear vector equally strong inclined to the vertical. In contrast, such waves generate strong vertical currents that may help maintain low N by moving water across large vertical distances, as suggested for deep water formation by Gascard (1973). We note that in our case these motions did not reach the surface where convective cooling occurs, and an additional (bottom stress) mixing source is needed to prevent any stratification from developing. We also note that Gascard's observations yielded strong w, which however were still only $w \sim 0.1u$. We expected that $w \sim u$ for gyroscopic waves. Thus, we need more detailed future observations using ADCP to resolve near-inertial shear and the vertical current component at the transition between $N = 0$ and $N \sim 2.5f$.

In the layers above 2200 m, the apparently prerequisite minimum internal gravity wave bandwidth including the first inertial harmonic suggested some internal wave generation mechanism like PSI being important. Excluding PSI as an important mechanism for tidal motions in the Algerian Basin, the particular value for minimum $N = 2.5f \approx 2\Omega + f$ seemed merely coincidental. Thus, the band $f < \sigma < 2f$ was not found special here, but may be so under different conditions (Garrett, 2001).

More likely, and not related to the above minimum value, internal gravity waves ($\sigma > f$) were generated through non-linear interactions. This was supported by the observed spectral fall-off rate of σ^{-3}: non-linear inertial-tidal interaction peaks were observed to fall off at the same rate in the Bay of Biscay (van Haren et al., 2002). In the Algerian Basin, where tides are weak, internal waves were more dominantly generated through interactions between near-inertial and sub-inertial motions. The latter were dominantly varying with

periods between 10–50 days. Such periods suggested that these motions were generated by passages of atmospheric disturbances. These disturbances possibly also generated bottom-trapped baroclinic topographic Rossby waves, considering some sub-inertial amplitude intensification at 2700 m.

The smooth transition in spectral continuum slope past the large scale $O(100\,\mathrm{m}$ vertically) $N(z)$ suggested that smaller scale (roughly estimated as <10 m vertically) stratification variations were important for observed occasional passages of higher frequency internal waves. This was especially clear at 1000 m around which the density profiles showed steps, explaining the spectral slope $p \approx -3$ and the spectral scaling by an average $N \approx 3f$, for $\sigma > 3f$. The passages of small layers of enhanced N were also occasionally observed around 1800 m, where $\sim 2f < N < \sim 3f$ (Fig. 2b), which could explain the continuation of the spectrum for $\sigma > 2.5f$ at this depth. In contrast, below 2200 m $p = -2$ and $N(z) = 0$ all the time, suggesting no support for internal gravity waves. At this depth 'only' gyroscopic waves were observed between $0 < \sigma < 2\Omega$, but dominantly between $0.97f < \sigma < 1.02f$. This points at trapping of sub-inertial motions ($0.97f < \sigma < f$) in the near-bottom layer. Our observations suggest that these deep Mediterranean near-inertial motions exist because of atmospheric disturbances passing above and because of specific reflection/transmission properties of different wave regimes, across transitions in stratification. This particular behavior demands further research, which should focus on such transition.

Acknowledgements

Financial support for the ELISA experiment was provided under the MAST3/MTP2/MATER EU program and shiptime was provided by IFREMER and INSU/CNRS. We thank all the participants in the ELISA campaigns and crews of R.V. 'Le Suroît', 'Thetys II' and 'Professeur Georges-Petit'. Isabelle Taupier-Letage provided Fig. 1. Margriet Hiehle Corel Drawed Figs. 3 and 8. We thank the anonymous reviewers for their comments. HvH thanks IFREMER for the hospitality during his stay in La Seyne-sur-mer, which was generously supported by a grant from the Netherlands organization for the advancement of scientific research, NWO, in the French-Dutch exchange program.

References

Albérola, C., Rousseau, S., Millot, C., Astraldi, M., Font, J., Garcia-Lafuente, J., Gasparini, G.P., Send, U., Vangriesheim, A., 1995. Tidal currents in the interior of the Western Mediterranean Sea. Oceanologica Acta 18, 273–284.

Brekhovskikh, L.M., Goncharov, V., 1994. Mechanics of Continua and Wave Dynamics. Springer, Berlin (342pp.).

D'Asaro, E.A., 1991. A strategy for investigating and modeling internal wave sources and sinks. In: Müller, P., Henderson, D. (Eds.), Dynamics of Oceanic Internal Gravity Waves, Proceedings 'Aha Huliko'a Hawaiian Winter Workshop. SOEST, Hawaii, pp. 451–465.

D'Asaro, E.A., Perkins, H., 1984. A near-inertial internal wave spectrum for the Sargasso Sea in late summer. Journal of Physical Oceanography 14, 489–505.

Davies, A.M., Xing, J., 2002. Influence of coastal fronts on near-inertial internal waves. Geophysical Research Letters 29 (23).

Eriksen, C.C., 1978. Measurements and models of fine structure, internal gravity waves, and wave breaking in the deep ocean. Journal of Geophysical Research 83, 2989–3009.

Fu, L.-L., 1981. Observations and models of inertial waves in the deep ocean. Review of Geophysics and Space Physics 19, 141–170.

Fuda, J.-L., Millot, C., Taupier-Letage, I., Send, U., Bocognano, J.M., 2000. XBT monitoring of a meridian section across the Western Mediterranean Sea. Deep-Sea Research I 47, 2191–2218.

Garrett, C., 2001. What is the "Near-Inertial" band and why is it different from the rest of the internal wave spectrum? Journal of Physical Oceanography 31, 962–971.

Garrett, C.J.R., Munk, W.H., 1972. Space–time scales of internal waves. Geophysical Fluid Dynamics 3, 225–264.

Gascard, J.-C., 1973. Vertical motions in a region of deep water formation. Deep-Sea Research 20, 1011–1027.

Gonella, J., 1972. A rotary-component method for analysing meteorological and oceanographic vector time series. Deep-Sea Research 19, 833–846.

Hibiya, T., Nagasawa, M., Niwa, Y., 2002. Nonlinear energy transfer within the oceanic internal wave spectrum at mid and high latitudes. Journal of Geophysical Research 107.

Kroll, J., 1975. The propagation of wind-generated inertial oscillations from the surface into the deep ocean. Journal of Marine Research 33, 15–51.

Kundu, P.K., 1993. On internal waves generated by travelling wind. Journal of Fluid Mechanics 254, 529–559.

Kunze, E., 1985. Near-inertial wave propagation in geostrophic shear. Journal of Physical Oceanography 15, 544–565.

Leaman, K.D., Sanford, T.B., 1975. Vertical propagation of inertial waves: a vector spectral analysis of velocity profiles. Journal of Geophysical Research 80, 1975–1978.

LeBlond, P.H., Mysak, L.A., 1978. Waves in the Ocean. Elsevier, Amsterdam (602pp.).

Maas, L.R.M., 2001. Wave focusing and ensuing mean flow due to symmetry breaking in rotating fluids. Journal of Fluid Mechanics 437, 13–28.

MEDOC Group, 1970. Observations of formation of deep water in the Mediterranean Sea, 1969. Nature 227, 1037–1040.

Millot, C., 1999. Circulation in the Western Mediterranean sea. Journal of Marine Systems 20, 423–442.

Millot, C., Crépon, M., 1981. Inertial oscillations on the continental shelf of the Gulf of Lions-Observations and theory. Journal of Physical Oceanography 11, 639–657.

Millot, C., Taupier-Letage, I., 2004. Additional evidence of LIW entrainment across the Algerian Basin by mesoscale eddies and not by a permanent westward flow. Journal of Geophysical Research, in press.

Millot, C., Taupier-Letage, I., Benzohra, M., 1997. Circulation off Algeria inferred from the Médiprod-5 current meters. Deep-Sea Research I 44, 1467–1495.

Mooers, C.N.K., 1975. Several effects of a baroclinic current on the cross-stream propagation of inertial-internal waves. Geophysical Fluid Dynamics 6, 245–275.

Munk, W., 1981. Internal waves and small-scale processes. In: Warren, B.A., Wunsch, C. (Eds.), Evolution of Physical Oceanography. MIT Press, Cambridge, pp. 264–291.

Nagasawa, M., Niwa, Y., Hibiya, T., 2000. Spatial and temporal distribution of the wind-induced internal wave energy available for deep water mixing in the North Pacific. Journal of Geophysical Research 105, 13,933–13,943.

Perkins, H., 1972. Inertial oscillations in the Mediterranean. Deep-Sea Research 19, 289–296.

Pinkel, R., 1983. Doppler sonar observations of internal waves: wave-field structure. Journal of Physical Oceanography 13, 804–815.

Pollard, R.T., Millard, R.C., 1970. Comparison between observed and simulated wind-generated inertial oscillations. Deep-Sea Research 17, 813–821.

Puillat, I., Taupier-Letage, I., Millot, C., 2002. Algerian eddies lifetimes can near 3 years. Journal of Marine Systems 31, 245–259.

Saint-Guily, B., 1970. On internal waves, effects of the horizontal component of the Earth's rotation and of a uniform current. Deutsches Hydrographisches Zeitschrift 23, 16–23.

Tsimplis, M.N., Proctor, R., Flather, R.A., 1995. A two-dimensional tidal model for the Mediterranean Sea. Journal of Geophysical Research 100, 16,223–16,239.

van Haren, H., 2000. Properties of vertical current shear across stratification in the North Sea. Journal of Marine Research 58, 465–491.

van Haren, H., 2004a. Incoherent internal tidal currents in the deep ocean. Ocean Dynamics 54, 66–76.

van Haren, H., 2004b. Bandwidth similarity at inertial and tidal frequencies in kinetic energy spectra from the Bay of Biscay. Deep-Sea Research I 51, 637–652.

van Haren, H., Maas, L., Zimmerman, J.T.F., Ridderinkhof, H., Malschaert, H., 1999. Strong inertial currents and marginal internal wave stability in the central North Sea. Geophysical Research Letters 26, 2993–2996.

van Haren , H., Maas, L., van Aken, H., 2002. On the nature of internal wave spectra near a continental slope. Geophysical Research Letters 29(12), 10.1029/2001GL014341. Corrigendum: 2003, 30(7), 1379, 10.1029/2003GL016952.

Visser, A.W., Souza, A.J., Hessner, K., Simpson, J.H., 1994. The effect of stratification on tidal current profiles in a region of freshwater influence. Oceanologica Acta 17, 369–381.

Xing, J., Davies, A.M., 2002. Processes influencing the non-linear interaction between inertial oscillations, near inertial internal waves and internal tides. Geophysical Research Letters 29 (5).

Webster, F., 1968. Observation of inertial period motions in the deep sea. Reviews of Geophysics 6, 473–490.